Hindawi
International Journal of Antennas and Propagation
Volume 2020, Article ID 3624563, 13 pages
https://doi.org/10.1155/2020/3624563

Research Article

A Novel Linear Sparse Array with Reconfigurable Pixel Antenna Elements

Ming Li,[1] Haiping Wei,[2] Jiahao Zhao,[1] Qingchang Tao ,[1] and Zheng You[1]

[1]*State Key Laboratory of Precision Measurement Technology and Instruments, Department of Precision Instrument, Tsinghua University, Beijing 100084, China*
[2]*National Key Laboratory of Science and Technology on Aerospace Intelligent Control, Beijing Aerospace Automatic Control Institute, Beijing 100854, China*

Correspondence should be addressed to Qingchang Tao; taoqingchang@mail.tsinghua.edu.cn

Received 20 January 2020; Accepted 1 April 2020; Published 23 April 2020

Academic Editor: Mohammod Ali

In this paper, on the basis of multifunctional reconfigurable pixel antenna (RPA) elements, a novel linear sparse array with an attractive compound reconfigurability is presented. It has the potential advantages of its beam scanning with low gain fluctuation, low sidelobe in two orthogonal planes, and polarization reconfigurable performance. Specifically, an RPA with simultaneous polarization and pattern reconstruction capabilities, consisting of the driven patch and the parasitic pixels on the same layer of dielectric substrate, is firstly designed, which can work in several operation modes corresponding to steerable beam directions ($\theta = 0^{\circ}$; θxoz = 25°, 45°; θyoz = 15°) with two circular polarizations in X-band. Cross-slot coupling feed is used to improve polarization reconstruction capability and reduce the complexity of hybrid reconstruction topology optimization. Then, those RPAs are integrated into the 1×8 linear sparse array to realize the reconfiguration of two circular polarizations and beam steering in *xoz*- and *yoz*-plane. Simulation results show that the gain fluctuation and sidelobe level of the array during beam scanning have significant advantages over the previous phased array, and the generation of antenna grating lobes is avoided. Moreover, both RPA element and RPA array prototypes have been fabricated and measured to testify the efficiency. The measured results agree well with the simulated ones, which indicates the application potential in the field of modern wireless communication system of the proposed linear sparse array.

1. Introduction

With the fast development of wireless technology rising the demand of the communication capacity, strict requirements have been raised and attached on the modern wireless communication system. As one of the most important components, antennas in the wireless communication systems are desired not only to integrate multifunction but also to have low size to save space and cost [1, 2]. Specifically, to cope with the ever-increasing demand of capacity, a high-gain intelligent antenna array is always expected, which is capable of steering its beam toward desired directions, while simultaneously placing nulls toward undesired directions of interferes, thereby enhancing the signal-to-noise ratio of the desired signal [3].

Reconfigurable antenna, that can achieve multiple antenna functions by modifying the physical structure or size in real-time, has recently gained considerable interests of researchers due to this intrinsic merit. Hence, reconfigurable antenna has become one promising candidate for high-gain, low-profile, and low-cost antennas [4]. Currently, some reconfigurable phased array antennas that can achieve high gain and beam scanning have been put forward [5, 6]. However, their reconfigurable performance has not been fully explored. In addition, due to the limitation of element factors, high sidelobe or even grating lobe is resulted for the reconfigurable phased array antenna when scanning at a large angle. To deal with this problem, the reconfigurable antenna element provides an effective solution. By its definition, we know that reconfigurable antennas can be

implemented either in the frequency, pattern, and polarization way or their combinations [7, 8]. Since frequency reconfigurable antennas allow frequency hopping and dynamically allocating spectrum, while radiation pattern and polarization reconfiguration can filter the in-band interference to increase the channel capacity, we think the compound reconfigurable antenna can be the right choice to address the drawbacks mentioned above existing in current reconfigurable phased array antennas. Then, the key problem becomes how to design reconfigurable antennas with individually tuning frequency, radiation pattern, and polarization [9–12].

To achieve compound reconfigurations, there are several issues to be considered. One tough issue is the compound or multiparameter reconfiguration that their strong interconnected relationship makes the reconfigurable antenna design becomes challenging. Currently, the extensively used approach of compound reconfiguration is to integrate different single-parameter reconfiguration techniques, which enables frequency-pattern reconfiguration [13], frequency-polarization reconfiguration [14], and pattern-polarization reconfiguration [15]. However, this method leads to a low reconfigurability and enables several operational modes with similar characteristics. To deal with this problem, another efficient candidate, i.e., pixel antenna has been put forward, which is considered to be one of the most flexible reconfigurable structures [16–23]. Pixel antenna divides the radiating surface into several small metal patches, namely, pixels, and interconnects them by means of RF-switches. Then, a patch is excited by coupling between the adjacent patches. By activating different switch configurations, the antenna surface is reshaped, thus reconfiguring its frequency and radiation characteristics.

Recently, pixel surfaces have already demonstrated its reconfigurable ability when used as the parasitic structures of the antenna, leading to significant advantages in the switch biasing, power handling, and integration possibilities [6, 24–26]. Nevertheless, the parasitic pixel layer is employed to realize single reconfiguration, without any further exploration in compound reconfigurable performance. Moreover, research on reconfigurable antenna arrays based on compound reconfigurable antenna elements has been less reported [27, 28].

In this paper, a novel linear sparse array with compound reconfigurability is presented. In order to realize the reconfiguration of array, the polarization and radiation pattern reconfigurable pixel antenna (RPA) is designed and optimized as the array element. The RPA consists of two layers, in which the parasitic layer with a grid of multisize patches is adopted as the top layer, and a metal ground with a cross gap is located between the upper and lower substrates. By controlling the topology of parasitic pixel layer and selecting different excitation ports, reconfigurability in beam steering and polarization of the proposed antenna can be achieved. Besides, the designed RPA element can produce varied modes of operation corresponding to steerable beam directions with two circular polarizations in X-band.

On the basis of RPA elements, a 1×8 linear array along the x-axis is presented. In order to realize the low sidelobe scanning and suppress the generation of grating lobe, nonuniform spacing is designed in the array structure and furthered optimized to reduce the coupling between array elements. Then, the low sidelobe beam scanning in xoz-plane and the beam deflection in the yoz-plane is realized due to the flexible performance of the pixel antenna element. In addition, the polarization reconfigurable performance of RPA is also retained in the array. Due to the advantages of the pattern and polarization compound reconfigurable, the proposed antenna can find broad applications in wireless communication.

2. RPA Structure and Optimization Design

2.1. Basic Structure Design. With the merit of flexible structure and high reconfiguration capability, pixel antenna divides the radiating surface into several small metal patches, called pixels. As shown in Figure 1, since the pixel patches closer to the feed port have a stronger influence over the input impedance of the antenna, it becomes important to balance the contribution of these pixels and switches to the reconfigurable performance. It also can be seen the larger patches are introduced with the increase of the distance from the port, which not only balances the influence of distance but also significantly reduces the number of switches and complexity.

In the pixel antenna design, the ultimate goal is to determine a clear relationship between the antenna geometry and its reconfigurable capability. Generally, the total size of the pixel surface(Lt) and the size of the pixel patch(Lp) can be estimated roughly by comparing with the wavelength [7, 8, 28]:

Since the length of the resonant paths has to be half the effective wavelength for the most restrictive frequency, we have

$$L_t > \left(\frac{\lambda_{low}}{2\sqrt{\varepsilon_{eff}}} \right), \tag{1}$$

where λlow is the free-space wavelength at the lowest frequency of operation and εeff is the effective permittivity of the pixel antenna.

To meet radiation pattern and frequency requirements, the total size has to be large enough while the individual pixel size has to be small enough to be able to finely tune the antenna properties. In addition, the pixel size is usually smaller than a tenth of a wavelength for the operation frequency, i.e.,

$$L_p > \left(\frac{\lambda_{\text{up}}}{10\sqrt{\varepsilon_{\text{eff}}}} \right), \tag{2}$$

where λup is the free-space wavelength at the highest frequency of operation.

The nonuniform size RPA proposed in this paper is shown in Figure 2, in which a double-layer substrate with different thickness is employed. The substrate selected is Rogers 5880 with $\varepsilon r = 2.2$. Notably, we take the symmetry axis of the two-port feedlines as the x-axis of the coordinate

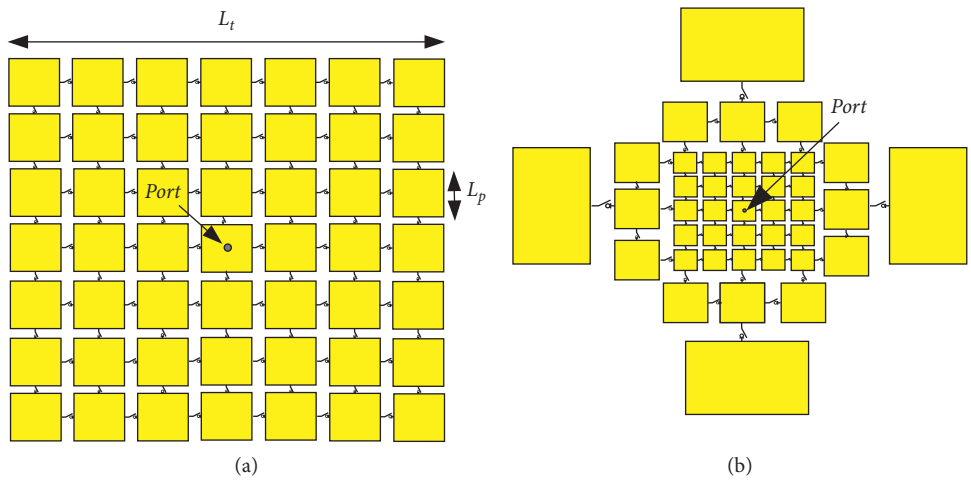

Figure 1: Schematic diagram of pixel antenna: (a) uniform pixel antenna; (b) multisize pixel antenna.

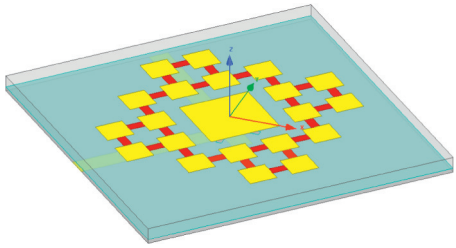

Figure 2: Configuration of the proposed RPA structure.

system. This ensures the symmetry of the antenna when changing the port feed. However, the direction of the feedlines is inclined 45° relative to the beam direction of the antenna (x-axis or y-axis), hence the substrate is set as a diamond to facilitate the installation of the SMA connector during testing.

The drive layer, the pixel parasitic layer, and the specific structure are shown in Figure 3. The thickness of the upper and the lower substrates is 1.524 mm and 0.508 mm, respectively. A metal ground with a cross gap is arranged between the two layers of substrates, and the aperture-coupled feed mechanism is introduced to improve the impedance matching and increase the impedance bandwidth of the antenna. The main components of the RPA architecture, the parasitic patch, is printed on the upper substrate with a symmetrical structure of nonuniform size. The width and length of the center patch can be calculated according to the basic theory of the pixel antenna. According to equation (2), Lp is 3.53 mm at 8.5 GHz and the pixel patch size of RPA in this paper is selected as 3.5 mm. Two loops of the pixel patch connected by the rectangular perfect electric conductor (PEC) are placed around the central patch. The geometric structure of the antenna can be changed by controlling the presence or absence of the PEC patch, which in turn changes the current distribution on the antenna, realizing the reconfiguration of the pattern. Two perpendicular microstrip feedlines are printed at the bottom of the drive layer and connected to two excitation ports respectively. By selecting different excitation port and switching states, the polarization reconfiguration under the same beam direction can be obtained. For convenience, the optimized geometrical parameters of the pixel antenna are provided in Table 1.

2.2. Topology Optimization. In this paper, due to its powerful searching ability and simple in the concept and implementation, the genetic algorithm (GA) in conjunction with HFSS is employed to determine the surface configurations of parasitic patches, i.e., switching states of the interconnections between adjacent pixel patches. For ease of analysis, the presence and absence of PEC patches are represented as 1 and 0, respectively, a binary array with a length of 24 is used as the variable to control the topological structure of the parasitic surface in the optimization process. When the optimization objective, i.e., the beam direction and the polarization performance of the RPA are satisfied, GA outputs the best binary array, and the final topological structure of RPA is obtained. The optimization method is detailed in [7], while the specific process is shown in Figure 4.

The optimized geometries and surface current distribution of the parasitic pixel surface with different feed ports are shown in Figure 5. Obviously, four steerable beam directions ($\theta = 0°; \theta\text{xoz} = 25°, 45°; \theta\text{yoz} = 15°$) with different polarizations are obtained.

When the topological structure in Figure 5(a) is selected and port 1 is excited, a 0° beam steering direction of the RPA with left-handed circular polarization (LHCP) mode is obtained. When exciting port 2, the structure and beam steering direction of the RPA do not change, while the main polarization mode of the antenna becomes right-handed circular polarization (RHCP). The beam steering directions of the topological structure of the RPA in Figure 5(b) and Figure 5(c) are 25° and45° in the xoz-plane, respectively. In that case, the main polarization mode of the RPA changes from LHCP to RHCP when the excited port is changed. Moreover, the beam steering direction of the topological structure of the RPA in Figure 5(d) is 15° in yoz-plane, and

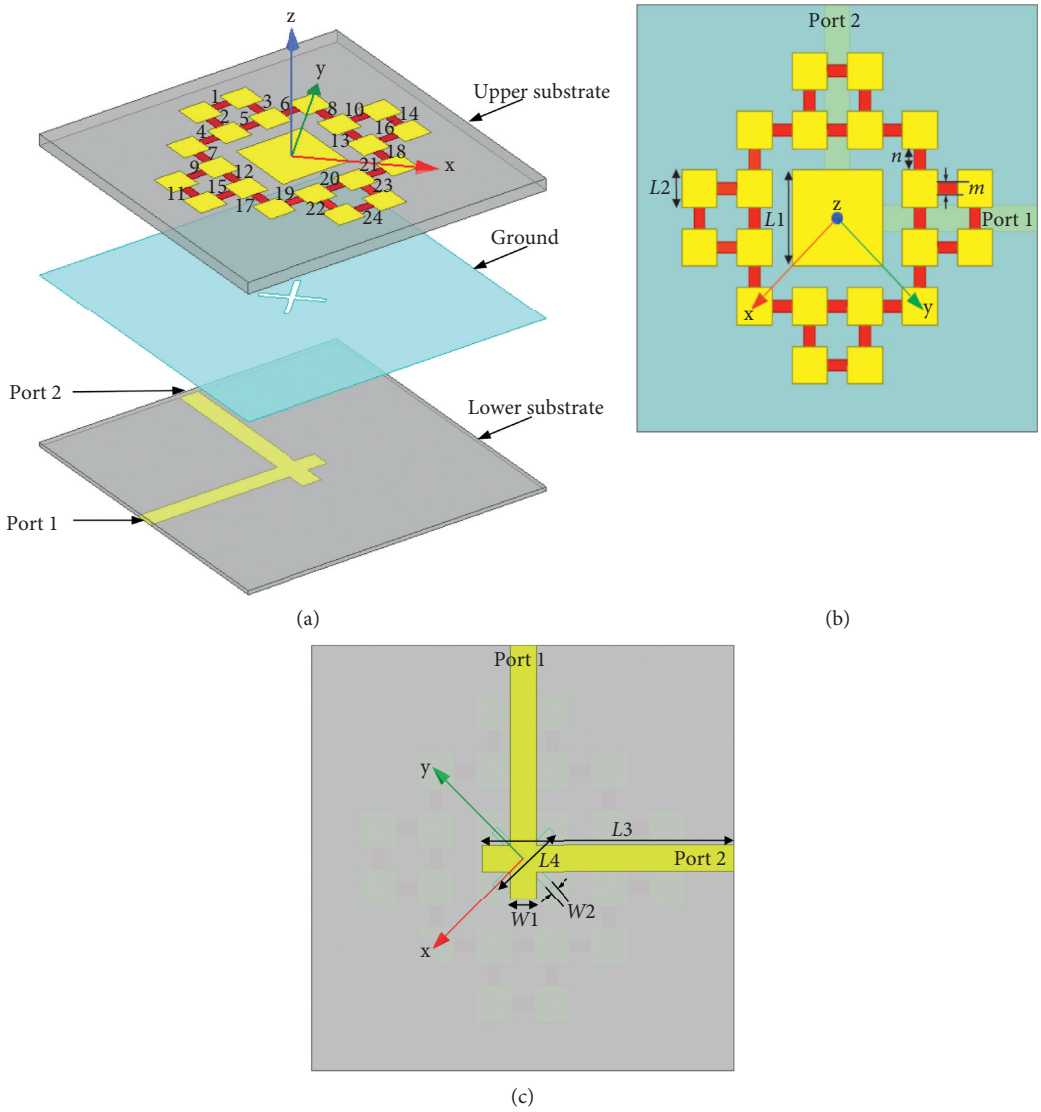

Figure 3: Multilayer structure of the RPA. (a) 3D structure. (b) Pixel parasitic layer (top view). (c) Driver layer (down view).

Table 1: Geometrical parameters of the RPA.

Parameter	*L1*	*L2*	*L3*	*L4*	*W1*	*W2*	*n*	*m*
Value (mm)	9	3.5	23.85	7.6	2.5	0.7	2.0	1.1

the main polarization mode of the RPA changes from LHCP to RHCP when changing the excited port from 1 to 2.

Figure 6 shows the corresponding simulated result of the RPAs shown in Figure 5. From Figure 6(a), it can be seen that with different parasitic layer topologies, the RPAs have an impedance bandwidth of 345.0 MHz covering the operating frequency of 8.5 GHz. It should be noted that, if extra switches are added between the driving patch and the pixel patches, the frequency reconfiguration performance can be achieved and the bandwidth can be further extended. Besides, it also can be seen from Figures 6(b), 6(c), and 6(d) that four modes of beam pointing and two modes of polarization can be obtained by choosing the different excitation port and topological structure.

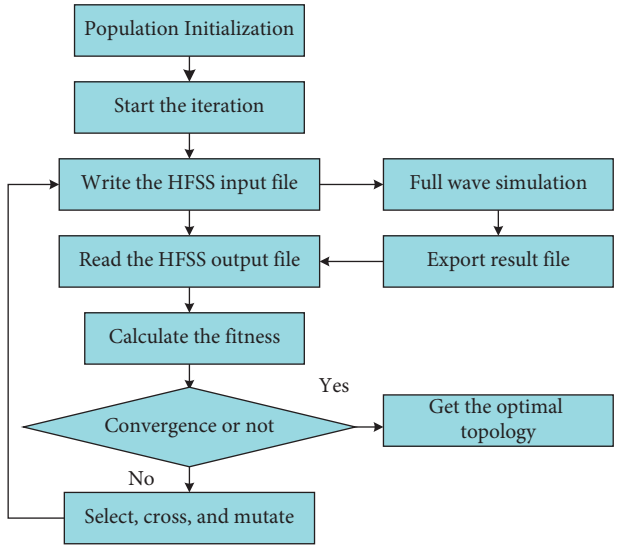

Figure 4: The topology optimization process of the RPA.

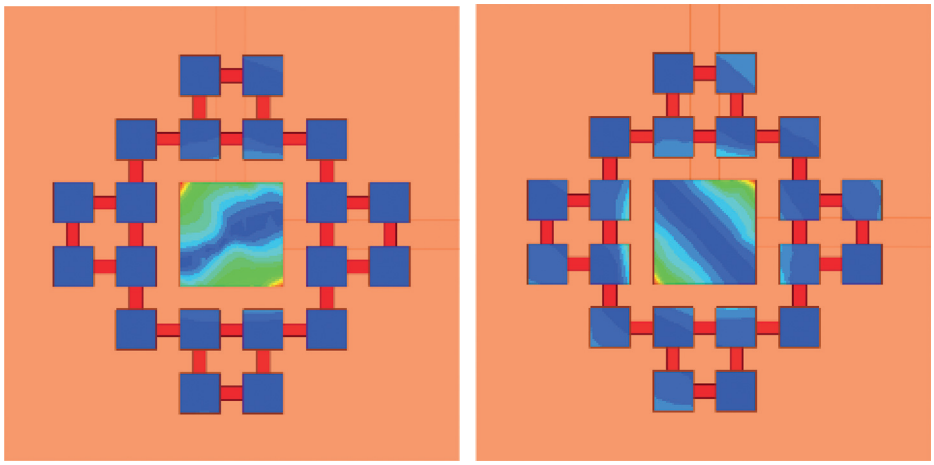

(a)

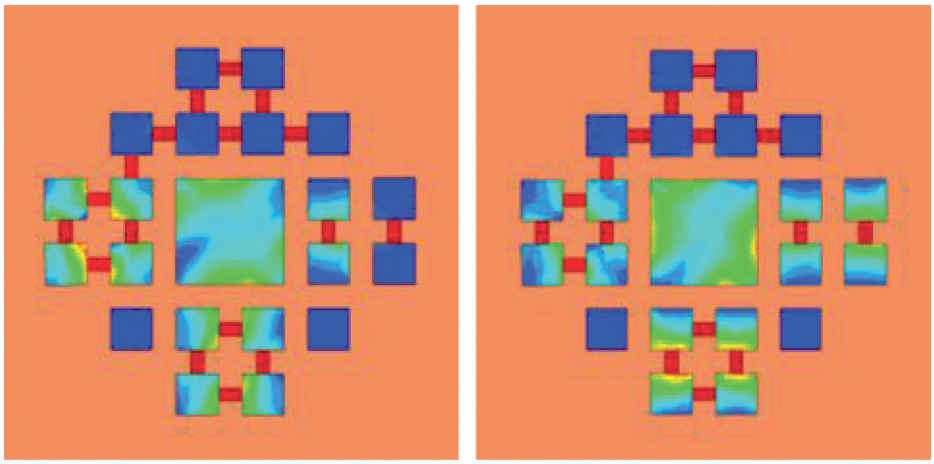

(b)

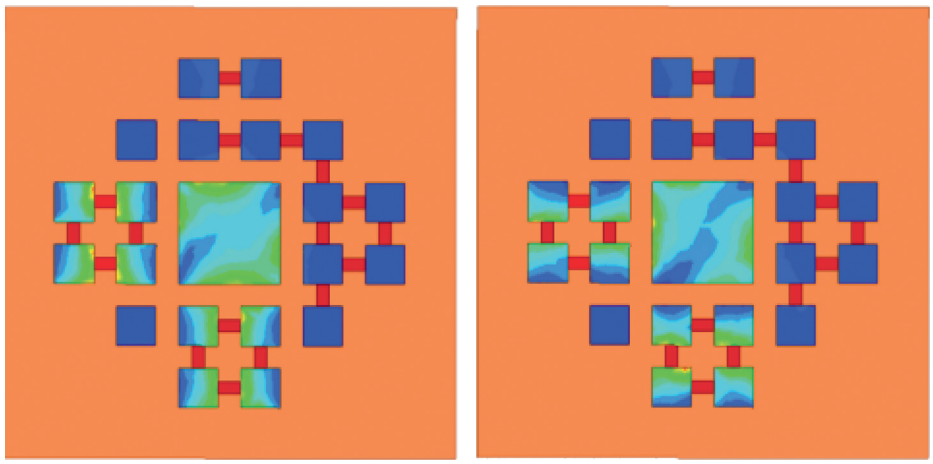

(c)

Figure 5: Continued.

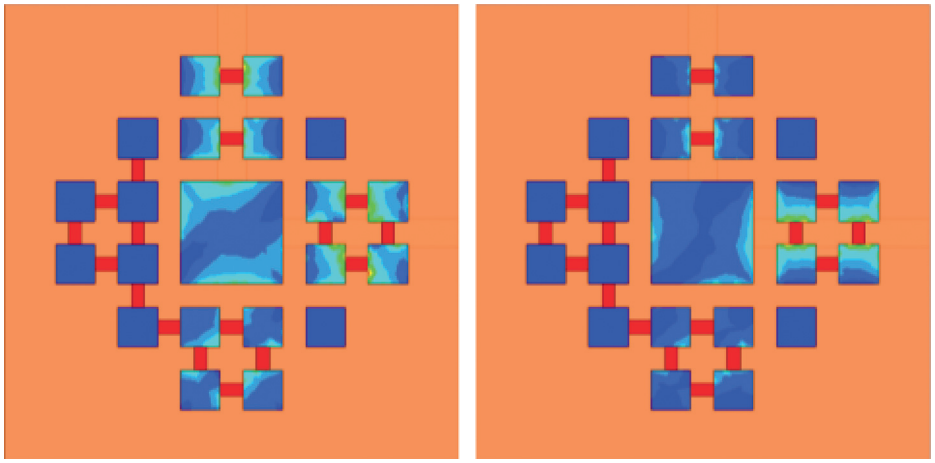

(d)

Figure 5: The optimized geometries and surface current distribution of the parasitic pixel surface with different feed ports. Beam steering direction. (a)$\theta = {}^{0^\circ}$. (b)θyoz = 25°. (c)θyoz = 45°. (d)θxoz = 15°.

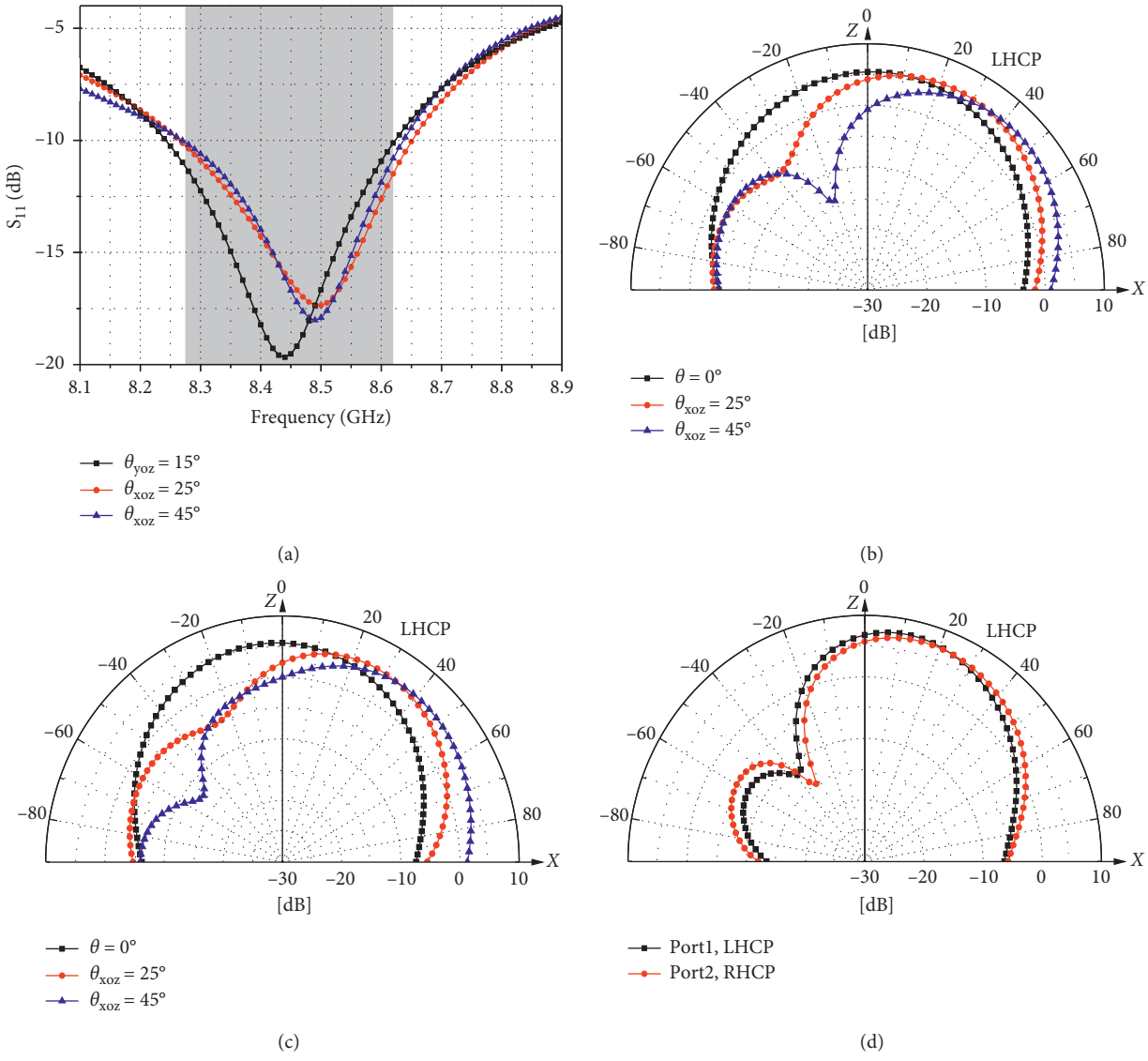

Figure 6: The simulated radiation patterns of different beam steering directions of the RPA. (a) S11. (b) *xoz*-plane, port 1. (c) *xoz*-plane, port 2. (d) *yoz*-plane.

3. RPA Array Design

3.1. Element Spacing Optimization. To further testify the superiority of RPA, a typical linear antenna array consisting of a number of RPA antenna elements is considered, where each element may be individually controlled in phase and amplitude, as shown in Figure 7.

At the far observation point P, the total field strength can be expressed as follows:

$$E_n = f(\theta, \varphi) \sum_{n=1}^{N} ane^{j\left((2\pi/\lambda)\mathrm{d}n\cos\theta\sin\varphi - \triangle\phi_B\right)}, \quad (3)$$

$$\Delta\phi B = \frac{2\pi}{\lambda}\mathrm{d}n\sin\theta\mathrm{B}, \quad (4)$$

where *an* represents the amplitude weighting coefficient of each array element, $\triangle\phi B$is the phase difference between adjacent elements, and θB indicates the beam steering direction of the antenna.

From equation (3), we know the pattern of antenna array consists of two parts, element factor$f_e(\theta, \varphi)$ and array factor$f_a(\theta, \varphi)$. Once the amplitude, phase, and spacing of elements are determined, the array factor is determined:

$$f(\theta, \varphi) = f_e(\theta, \varphi) \times f_a(\theta, \varphi). \quad (5)$$

When the number of elements, excitations, and spacing of elements are determined, the array factor is determined. In that case, a different element factor pattern will affect the array radiation properties. For the conventional phased array, monopole, waveguide gap, and microstrip patch are always used as the elements. However, these antennas have the drawback of single beam pointing, and a degradation in the gain can be caused with the increase of the angle. This correspondingly results in a large gain fluctuation in the beam scanning, and it is easy to generate a grating lobe in the scanning of the large angle.

In this paper, the RPA is designed to realize the reconfiguration of polarization and radiation pattern. The pattern reconfigurable performance enables the antenna to cover a wide range of angles with a high and stable gain by changing beam pointing, as seen in Figures 6(b) and 6(c), verifying that RPA can achieve the beam scanning with a small gain fluctuation.

Unfortunately, the problem of grating lobe suppression is not solved yet. To deal with this problem, the sparse distribution technology provides an efficient candidate to reduce the sidelobe level of the array. Nonetheless, instead of using the sparse array with the isotropic element, the antenna array designed in this paper adopts RPA as the array element, and the coupling between the array elements is considered in the calculation process of the array pattern. To optimize array spacing, the active element pattern and improved fruit-fly optimization algorithm (FOA) are introduced [29]. The optimization steps are briefly provided as follows:

(1) Builds the RPA array model and extracts the active pattern of each element

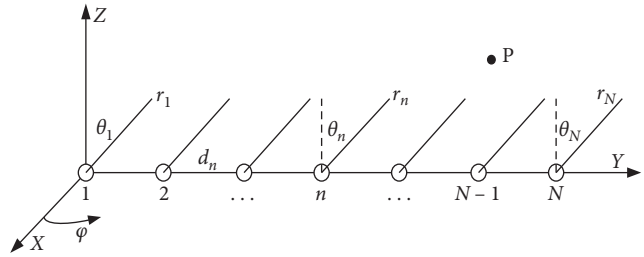

Figure 7: Schematic diagram of the linear array antenna.

(2) Initializes the optimization parameters and starts the iterative process

(3) Calculates the array pattern and determines whether it satisfies the terminal criterion

(4) If satisfied, outputs the final solution; otherwise continues to iterate.

To clarify this process, we construct an antenna array by a linear combination of eight identical optimized RPA elements arranged along the *x*-axis. Then, the optimization variable can be denoted as $\mathbf{d} = [d1, d2, ..., di, ..., d7]$, where*di* is the spacing between the *i*-th and the (*i*+1)-th element. For convenience, the objective function is listed in equation (5). The optimization interval of the element spacing is $0.8\lambda - 1.1\lambda$ at the resonant frequency of 8.5 GHz:

$$\min_{\mathbf{d}} \max[\max \mathrm{HPBW}(\mathbf{d}), 15] + \max[\max \mathrm{SLL}(\mathbf{d}), -15],$$
$$s.t. \quad \mathbf{d} = [d1, d2, ..., di, ..., d7], \quad di \in (0.8\lambda, 1.1\lambda), \quad (6)$$

where $\max \mathrm{SLL}(\mathbf{d})$ and $\max \mathrm{HPBW}(\mathbf{d})$ are the maximum sidelobe level and the maximum half power beam width of the array pattern, respectively, with the specific scanning angles. In this section, we assume that the optimal target of the sidelobe level and beam width are −15 dB and 15°, respectively. For convenience, the optimized element spacing is provided in Table 2.

3.2. RPA Array Steering in the xoz-Plane. Figure 8 shows the schematic of the 1 × 8 RPA array. Without loss of generality, we assume the feeding network is scanned with a direction of 25° and 45° in the *xoz*-plane, respectively. In order to prevent the distortion of the pattern, a parallel symmetrical feeding network is designed, and the polarization reconfiguration can be realized at the same angle by changing the feed port. The equal amplitude feeding network is located at the driving layer of the antenna array, and the two assembled arrays are simulated.

The simulation results of the two arrays are shown in Figure 9 and Figure 10. The radiation performance of the two arrays under different port excitation is shown in Table 3. As can be seen, when port 1 is excited, the main beam directions of the two arrays are 25° and45°, and LHCP polarization mode is achieved. The SLL of the two arrays are −15.9 dB and −15.5 dB separately. By changing the feed port, the polarization mode changes to RHCP correspondingly, and the

Table 2: Element spacing of the RPA array.

Element no.	*d1*	*d2*	*d3*	*d4*	*d5*	*d6*	*d7*
Spacing (mm)	31.83	32.41	29.98	29.98	29.98	29.98	47.77

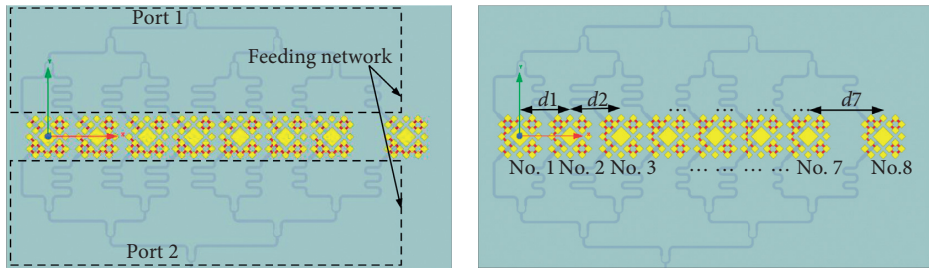

Figure 8: The schematic of the 1 × 8 linear array with feeding network. (a) $\theta xoz = 25^{\circ}$. (b) $\theta xoz = 45^{\circ}$.

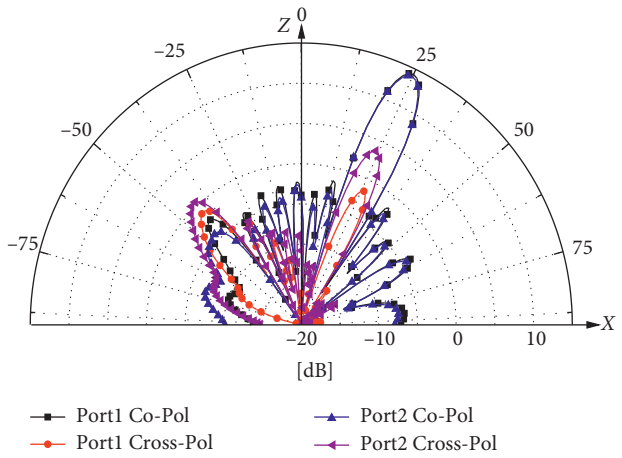

Figure 9: Simulated radiation pattern with the beam steering angles of $\theta xoz = 25^{\circ}$.

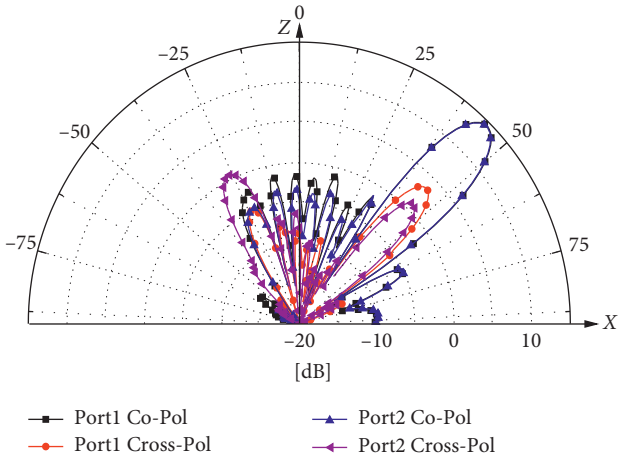

Figure 10: Simulated radiation pattern with the beam steering angles of $\theta xoz = 45^{\circ}$.

Table 3: Radiation performance of the RPA array.

Angle	$\theta_{xoz} = 25^{\circ}$		$\theta_{xoz} = 45^{\circ}$	
Port	Port 1	Port 2	Port 1	Port 2
Gain (dB)	14.3	14.0	14.5	14.4
SLL (dB)	−15.9	−16.5	−15.5	−15.8
HPBW (°)	7.6	7.7	9.8	9.8
Pol_Mode	LHCP	RHCP	LHCP	RHCP

SLLs are -16.5 dB and −15.8 dB, respectively. Compared with the optimization objective, the sidelobe of the array with a scanning angle of 45° was increased by 0.7 dB at port 2, but this is acceptable because the loss of the feed network would inevitably affect the radiation performance of the array. Under different reconfigurability states, the gain of antenna array fluctuates less than 0.5 dB. Therefore, the optimization objective is well achieved on the whole.

In order to verify the advantages of RPA array in suppressing grating lobe and reducing gain fluctuation, two additional arrays, i.e., uniform array of RPA elements (array (a)) and sparse array of non-reconfigurable element (array (b)), are designed for comparison, respectively. Each element spacing *di* is 33.14 mm of array (a). In array (b), the RPA with the beam steering angles of 0° is assumed. For fair comparison, the apertures of arrays (a) and (b) are the same as those of the designed array described above.

The simulated results of uniform and sparse arrays are shown in Figures 11 and 12, respectively. As shown in Figure 11, it can be seen that compared with the nonuniform array, the sidelobe level increases by about 3 to 5 dB in uniform array when scanning to 25° and 45°. The grating lobe begins to appear as shown in Figure 12. Figure 13 shows the gain fluctuation and SLL contrast between the two arrays and the RPA array proposed in this paper. We can see that the array presented in this paper has obvious advantages in reducing gain fluctuation, suppressing the sidelobe level, and avoiding the grating lobe.

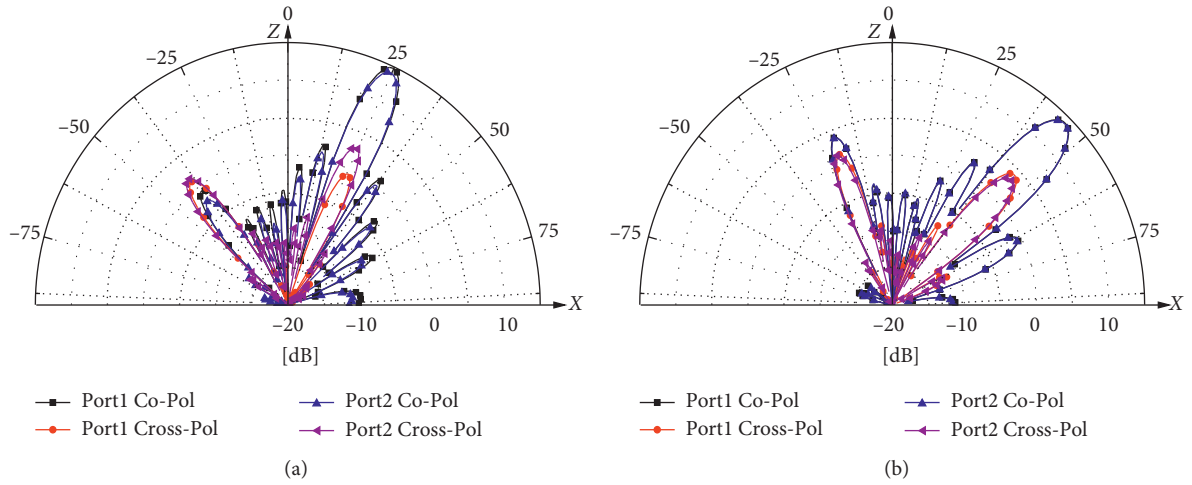

Figure 11: Simulated radiation pattern of the array. (a) $\theta xoz = 25^{\circ}$. (b) $\theta xoz = 45^{\circ}$.

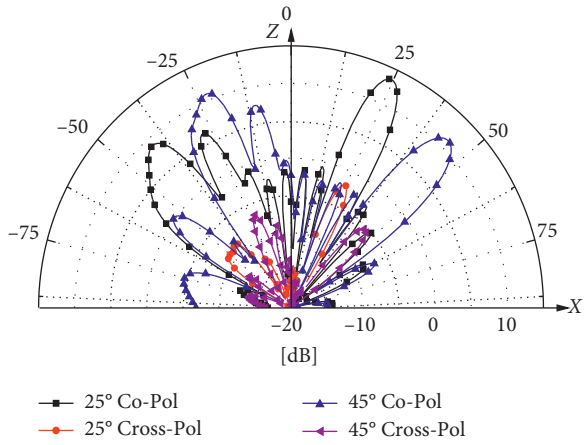

Figure 12: Simulated radiation pattern of the array (b), Port 1.

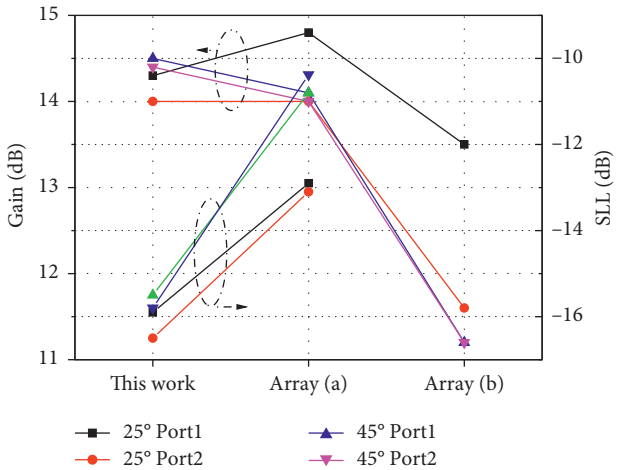

Figure 13: Gain fluctuation and SLL of three classes of arrays.

3.3. RPA Array Steering in the yoz-Plane. For the array composed of RPA whose beam steering direction is fixed in *yoz*-plane, the steering direction of the array pattern is only related to the element factor since the beam steering in *yoz*-plane is accomplished by the beam-steering capabilities of the individual RPAs of the array. As a result, the phase front always stays parallel to the *x*-axis and there is no need to employ phase shifters. To demonstrate this fact, an array is formed by the RPA designed in Section 2 with a 15° beam deflection in *yoz*-plane. The aperture of this array is the same as the optimized aperture of the array mentioned in Figure 8. Figure 14 show its simulation results.

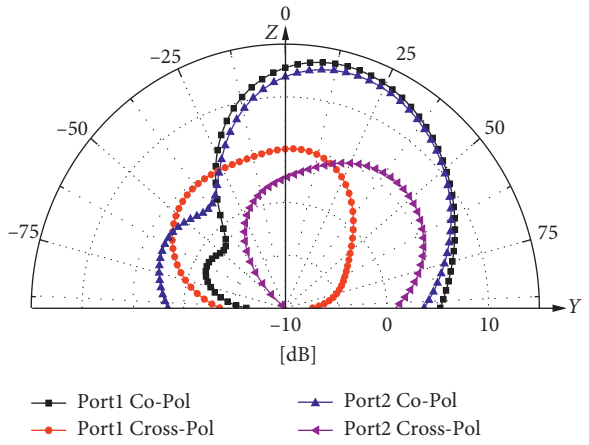

Figure 14: Simulated radiation pattern with the beam steering angles of θyoz = 15° in *yoz*-plane.

From Figure 14, it can be seen that the main beam direction of the RPA array is 15° in the *xoz*-plane. When port 1 is excited, LHCP main polarization mode with a gain of 13.7 dB is resulted. When the port 2 is excited, RHCP main polarization mode is obtained, owing a gain of 13.1 dB.

4. Fabrication and Measurement

To verify the superiority, both RPAs and RPA arrays with beam steering in the *yoz*-plane have been fabricated.

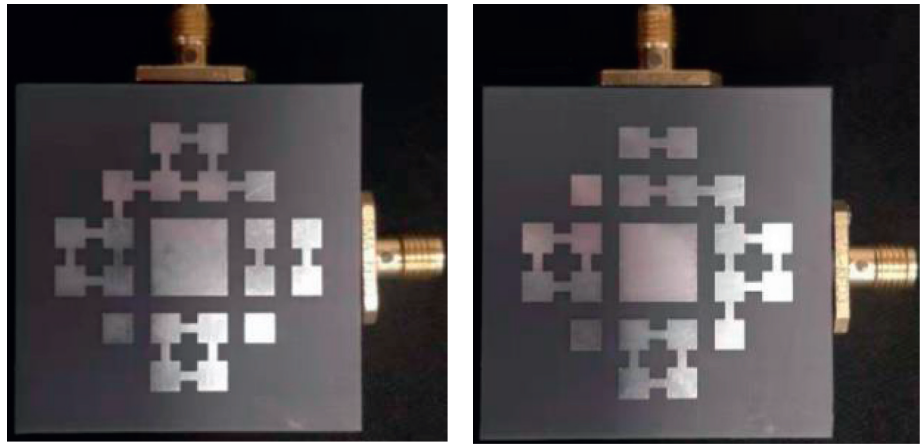

(a) (b)

Figure 15: The fabricated RPA prototype. (a) θxoz = 25°. (b) θxoz = 45°.

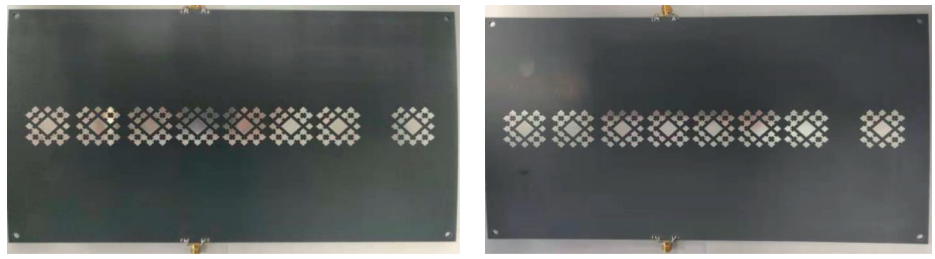

(a) (b)

Figure 16: The fabricated 1×8 linear array prototype. (a) θxoz = 25°. (b) θxoz = 45°.

Figure 17: The measured scene.

Figure 15 and Figure 16 show the fabricated RPAs and arrays prototype, respectively.

The radiation pattern measurement setup is shown in Figure 17. Figures 18, 19, and 20, respectively, show the measured results of the reflection coefficient, radiation pattern of the RPA, and the radiation pattern of the array. It can be seen from Figures 18 and 19 that the impedance bandwidth of the fabricated RPAs is greater than 200.0 MHz covering the operating frequency of 8.5 GHz, and the exact beam pointing is obtained. From Figure 20, due to the amplitude and phase errors of the antenna feeding network and production and test errors, the sidelobe level of the fabricated arrays is slightly increased but maintained below −11.5 dB. For the four reconstruction states in Figure 20, antenna gains are 11.7 dB, 11.2 dB, 11.5 dB, and 11.0 dB, respectively. The gain fluctuation of antenna array is less than 1.0 dB. On the whole, the simulated and measured results are in good agreement.

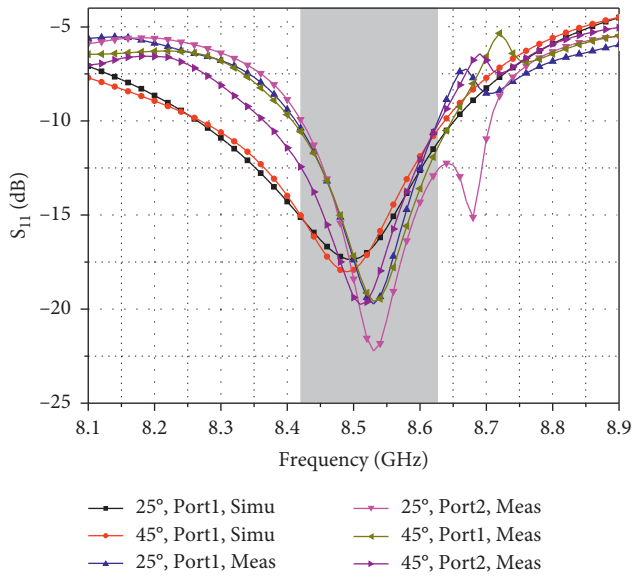

Figure 18: The S_{11} measured result of different beam steering direction of the RPA prototype.

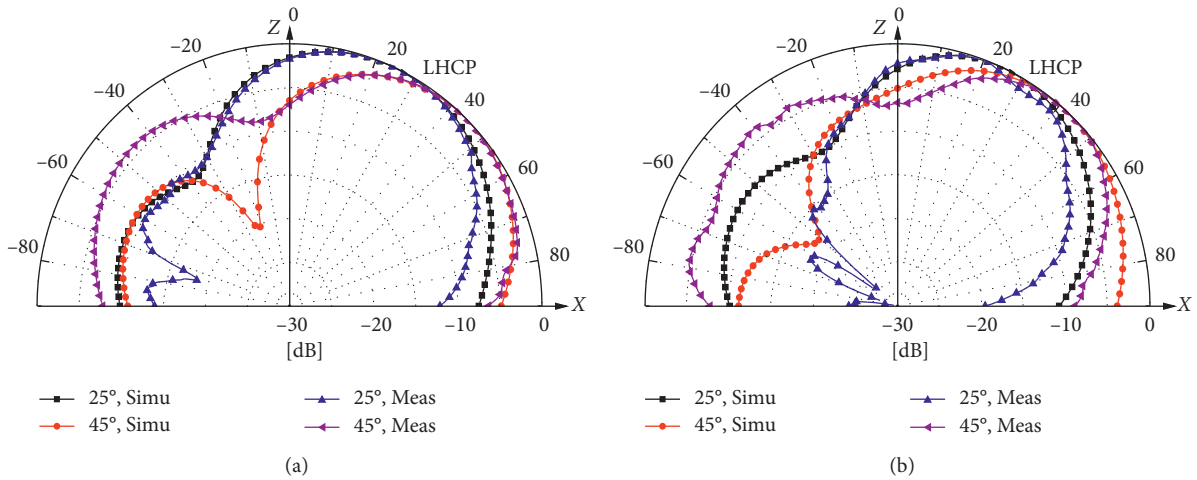

Figure 19: The normalized radiation pattern measured results of different ports of the RPA prototype. (a) Port 1. (b) Port 2.

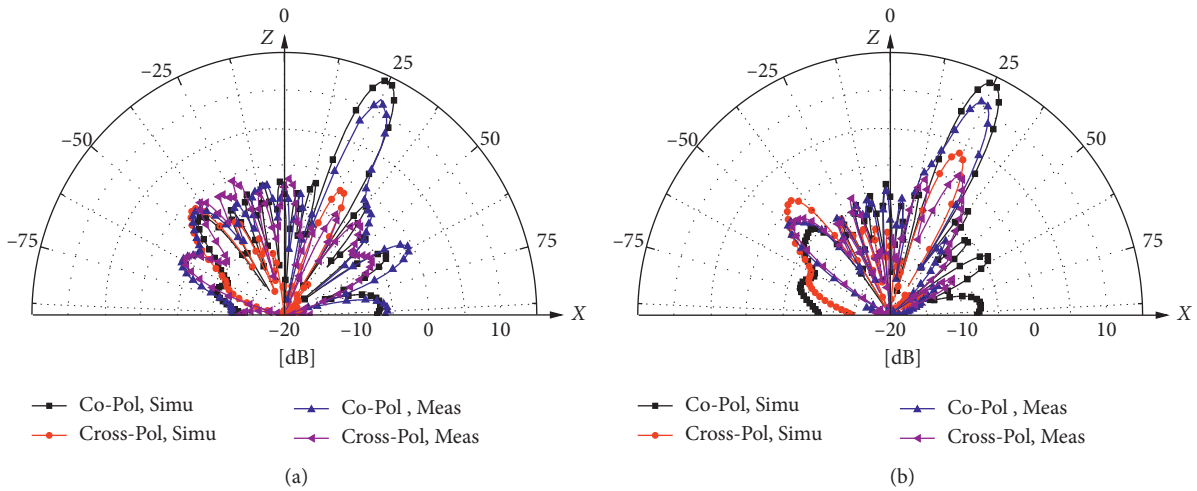

Figure 20: Continued.

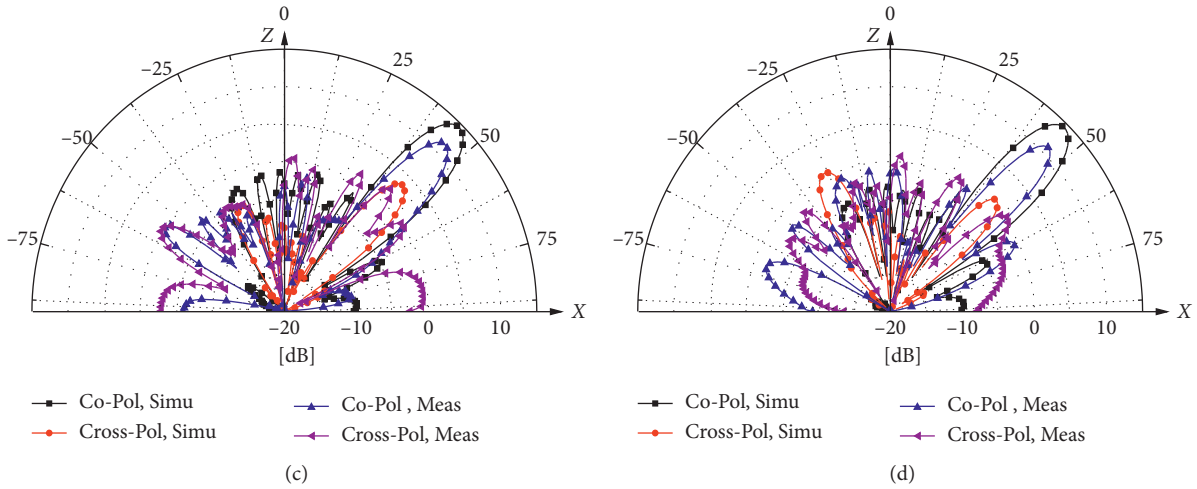

Figure 20: Measured radiation pattern with the different beam steering angles and feed ports. (a) $\theta xoz = 25^{\circ}$, Port 1; (b) θxoz = 25°, Port 2; (c) θxoz = 45°, Port 1; (d) θxoz = 45°, Port 2.

Table 4: Radiation performance of the RPA array.

Item	This work	Ref. [27]	Ref. [28]	Ref. [30]
Reconfiguration	Polarization and pattern	Frequency, polarization, and pattern (not independent)	Pattern	Frequency and pattern
Array	1 × 8	1 × 2	1 × 4	9 × 8
Arrangement of elements	Sparse	Uniform	Uniform	Uniform
Maximum scanning range (°)	45	30 (antenna element)	30	60
Gain fluctuation (dB)	<1.0	Not mentioned	±0.2	3.0–5.0
SSL (dB)	<−15.0	Not mentioned	<−8.5	<−10.0@45°

At the same time, Table 4 lists the comparison of the linear sparse hybrid reconfigurable antenna array proposed in this paper with other designs. It can be seen that the work of this paper has obvious comprehensive advantages in terms of antenna scanning angle and scanning dimension, especially antenna gain fluctuation and sidelobe level in the large-angle scanning state.

5. Conclusion

In this paper, a novel linear sparse array with compound reconfigurability has been proposed. The proposed antenna array is constructed by the linear combination of identical multifunctional reconfigurable pixel antenna elements, which is motivated by the fascinating characteristic that each RPA produces varied modes of operation corresponding to steerable beam directions with two different circular polarizations in X-band, thus an important additional degree of freedom has been introduced into the array design. Then, with the help of population intelligence optimization, the 1 × 8 nonuniform linear array has been designed. Compared with the traditional phased array, the designed array not only can achieve polarization reconfiguration but also can significantly suppress the appearance of grating lobe and greatly reduce the gain fluctuation during beam scanning. Even without amplitude weighting, the sidelobe level of the reconfigurable antenna array for large-angle scanning is less than -15 dB and the gain fluctuation is even less than 1.0 dB. Finally, the prototypes of RPA and RPA array have been fabricated and measured. The measured and simulated results agree well, indicating that the designed antenna can achieve the beam scanning with low gain fluctuation, low sidelobe in two orthogonal planes, and good polarization reconfigurable performance.

Data Availability

The data used to support the findings of this study are included within the article.

Conflicts of Interest

The authors declare that there are no conflicts of interest regarding the publication of this paper.

Acknowledgments

This work was supported by the National Natural Science Foundation of China under Grant 61774096.

References

[1] C. M. Lee and C. W. Jung, "Radiation-pattern-reconfigurable antenna using monopole-loop for fitbit flex wristband," *IEEE*

Antennas and Wireless Propagation Letters, vol. 14, pp. 269–272, 2015.

[2] T. Ben, H. Rmili, and M. , "Design of reconfigurable radiation pattern ring-dipole antenna for wireless communication," in *Proceedings of the 2013 7th European Conference on Antennas and Propagation (EuCAP)*, vol. 1252–1255, EuCAP, Gothenburg, Sweden, April 2013.

[3] Y. Cai, Y. J. Guo, and A. R. Weily, "A frequency-reconfigurable quasi-yagi dipole antenna," *IEEE Antennas and Wireless Propagation Letters*, vol. 9, pp. 883–886, 2010.

[4] L. Randy, "Haupt and michael lanagan, "reconfigurable antennas," *IEEE Antennas and Propagation Magazine*, vol. 55, no. 1, 2013.

[5] J. Zhang, S. Zhang, A. S. Morris, and G. F. Pedersen, "Radiation-pattern reconfigurable phased array with p-i-n diodes controlled for 5G mobile terminals," *IEEE Transactions on Microwave Theory and Techniques*, vol. 68, no. 3, pp. 1–15, 2020.

[6] P. K. Li, Z. H. Shao, Q. Wang, and Y. J. Cheng, "Frequency- and pattern-reconfigurable antenna for multistandard wireless applications," *IEEE Antennas and Wireless Propagation Letters*, vol. 14, pp. 333–336, 2015.

[7] X. Yuan, Z. Li, D. Rodrigo et al., "A parasitic layer-based reconfigurable antenna design by multi-objective optimization," *IEEE Transactions on Antennas and Propagation*, vol. 60, no. 6, pp. 2690–2701, 2012.

[8] Z. Li, E. Ahmed, A. M. Eltawil, and B. A. Cetiner, "A beam-steering reconfigurable antenna for WLAN applications," *IEEE Transactions on Antennas and Propagation*, vol. 63, no. 1, pp. 24–32, 2015.

[9] M. A. Towfiq, I. Bahceci, S. Blanch, J. Romeu, L. Jofre, and B. A. Cetiner, "A reconfigurable antenna with beam steering and beamwidth variability for wireless communications," *IEEE Transactions on Antennas and Propagation*, vol. 66, no. 10, pp. 5052–5063, 2018.

[10] P.-Y. Qin, F. Wei, and Y. J. Guo, "A wideband-to-narrowband tunable antenna using a reconfigurable filter," *IEEE Transactions on Antennas and Propagation*, vol. 63, no. 5, pp. 2282–2285, 2015.

[11] M. Mirmozafari, G. Zhang, S. Saeedi, and R. J. Doviak, "A dual linear polarization highly isolated crossed dipole antenna for MPAR application," *IEEE Antennas and Wireless Propagation Letters*, vol. 16, pp. 1879–1882, 2017.

[12] W.-Q. Wang, "Inflight antenna pattern measurement for bistatic synthetic aperture radar systems," *IEEE Antennas And Wireless Propagation Letters*, vol. 6, pp. 432–435, 2007.

[13] T. Aboufoul, K. Ali, A. Alomainy, and C. Parini, "Combined pattern and frequency reconfiguration of single-element ultra-wideband monopole antenna for cognitive radio devices," in *Proceedings of the 2013 7th European Conference On Antennas And Propagation*, EuCAP), Gothenburg, Sweden, pp. 932–936, April 2013.

[14] Y. B. Dhanade and Y. K. Choukiker, "Frequency and polarization reconfigurable antenna for wireless communication," in *Proceedings of the 2017 International Conference of Electronics*, Communication and Aerospace Technology (ICECA), London, UK, pp. 287–290, July 2017.

[15] A. Chen, X. Ning, L. Wang, and Z. Zhang, "A design of radiation pattern and polarization reconfigurable antenna using metasurface," in *Proceedings of the 2017 IEEE Asia Pacific Microwave Conference*, vol. 108-111, IEEE, Kuala Lumpur, Malaysia, February 2017.

[16] B. A. Cetiner, H. Jafarkhani, J. Y. Qian, and H. J. Yoo, "Multifunctional reconfigurable MEMS integrated antennas for adaptive MIMO systems," *IEEE Communications Magazine*, vol. 42, no. 12, pp. 62–70, 2004.

[17] B. A. Cetiner, E. Akay, E. Sengul, and E. Ayanoglu, "A MIMO system with multifunctional reconfigurable antennas," *IEEE Antennas and Wireless Propagation Letters*, vol. 5, pp. 463–466, 2006.

[18] D. Rodrigo, Y. Damgaci, N. Biyikli, B. A. Cetiner, J. Romeu, and L. Jofre, "MEMS-reconfigurable antenna based on a multi-size pixelled geometry," in *Proceedings of the Fourth European Conference on Antennas and Propagation, Barcelona, Spain*, pp. 1–4, 2010.

[19] D. Rodrigo, B. A. Cetiner, and L. Jofre, "Frequency, radiation pattern and polarization reconfigurable antenna using a parasitic pixel layer," *IEEE Transactions on Antennas and Propagation*, vol. 62, no. 6, pp. 3422–3427, 2014.

[20] D. Rodrigo and L. Jofre, "Frequency and radiation pattern reconfigurability of a multi-size pixel antenna," *IEEE Transactions on Antennas and Propagation*, vol. 60, no. 5, pp. 2219–2225, 2012.

[21] C.-Y. Chiu, J. Li, S. Song, and R. D. Murch, "Frequency-reconfigurable pixel slot antenna," *IEEE Transactions on Antennas and Propagation*, vol. 60, no. 10, pp. 4921–4924, 2012.

[22] P. Lotfi, S. Soltani, and R. D. Murch, "Printed endfire beam-steerable pixel antenna," *IEEE Transactions on Antennas and Propagation*, vol. 65, no. 8, pp. 3913–3923, 2017.

[23] S. Soltani, P. Lotfi, and R. D. Murch, "Design and optimization of multiport pixel antennas," *IEEE Transactions on Antennas And Propagation*, vol. 66, no. 4, pp. 2049–2054, 2018.

[24] J. C. Myers, P. Chahal, E. Rothwell, and L. Kempel, "A multilayered metamaterial-inspired miniaturized dynamically tunable antenna," *IEEE Transactions on Antennas and Propagation*, vol. 63, no. 4, pp. 1546–1553, 2015.

[25] A. Grau Besoli and F. De Flaviis, "A multifunctional reconfigurable pixeled antenna using MEMS technology on printed circuit board," *IEEE Transactions on Antennas and Propagation*, vol. 59, no. 12, pp. 4413–4424, 2011.

[26] S. Song and R. D. Murch, "An efficient approach for optimizing frequency reconfigurable pixel antennas using genetic algorithms," *IEEE Transactions on Antennas and Propagation*, vol. 62, no. 2, pp. 609–620, 2014.

[27] Y. P. Selvam, M. Kanagasabai, G. N. Alsath et al., "A patch-slot antenna array with compound reconfiguration," *IEEE Antennas Wireless Propagation Letters*, vol. 17, no. 3, pp. 525–528, 2018.

[28] Z. Li, D. Rodrigo, L. Jofre, and B. A. Cetiner, "A new class of antenna array with a reconfigurable element factor," *IEEE Transactions on Antennas and Propagation*, vol. 61, no. 4, pp. 1947–1955, 2013.

[29] A. Darvish and A. Ebrahimzadeh, "Improved fruit-fly optimization algorithm and its applications in antenna arrays synthesis," *IEEE Transactions on Antennas and Propagation*, vol. 66, no. 4, pp. 1756–1766, 2018.

[30] N. Haider, A. G. Yarovoy, and A. G. Roederer, "L/S-band frequency reconfigurable multiscale phased array antenna with wide angle scanning," *IEEE Transactions on Antennas and Propagation*, vol. 65, no. 9, pp. 4519–4528, 2017.